Medical Engineering and Physics 68 (2019) 76–84

Contents lists available at ScienceDirect

Medical Engineering and Physics

journal homepage: www.elsevier.com/locate/medengphy

On the axial distribution of plaque stress: Influence of stenosis severity, lipid core stiffness, lipid core length and fibrous cap stiffness

César Alegre-Martínez[a], Kwing-So Choi[a], Outi Tammisola[a,b], Donal McNally[a,*]

[a] Faculty of Engineering, University of Nottingham, Nottingham, United Kingdom
[b] KTH Mechanics, KTH Royal Institute of Technology, Stockholm, Sweden

ARTICLE INFO

Article history:
Received 7 February 2018
Revised 12 February 2019
Accepted 25 February 2019

Keywords:
Stenotic flow
Fluid-structure interaction
Elastic wall
Atherosclerosis
Plaque rupture

ABSTRACT

Numerical simulations of blood flow through a partially-blocked axisymmetric artery are performed to investigate the stress distributions in the plaque. We show that the combined effect of stenosis severity and the stiffness of the lipid core can drastically change the axial stress distribution, strongly affecting the potential sites of plaque rupture. The core stiffness is also an important factor when assessing plaque vulnerability, where a mild stenosis with a lipid-filled core presents higher stress levels than a severe stenosis with a calcified plaque. A shorter lipid core gives rise to an increase in the stress levels. However, the fibrous cap stiffness does not influence the stress distributions for the range of values considered in this work. Based on these mechanical analyses, we identify potential sites of rupture in the axial direction for each case: the midpoints of the upstream and downstream regions of the stenosis (for severe, lipid-filled plaques), the ends of the lipid core (for short cores), and the middle of the stenosis (for mild stenoses with positive remodelling of the arterial wall).

1. Introduction

Atherosclerosis is a cardiovascular disease that remains the most common cause of death in Western countries [1]. It consists of the narrowing of an artery due to the accumulation of fatty substances in the inner layer [2,3]. This accumulation is known as a plaque. The rupture of the covering of the plaque is a dangerous condition, which may finally lead to a stroke, or a myocardial infarction [4]. Hence, it is important to identify the plaques that are most likely to rupture and why. While the mechanisms behind disease initiation, progression and rupture are diverse [1,5], here we aim to perform a study to analyse the mechanical aspects of the plaque rupture process. In particular, some geometrical features such as the severity of the stenosis or the length of the lipid core will be studied, along with other parameters such as the stiffness of the lipid core.

Early studies such as the one performed by Richardson et al. investigated the locations of plaque rupture in coronary arteries [6]. Using 71 cross-sectional samples of atherosclerotic arteries with a lipid core, they found that in 59% of the cases the rupture took place at the shoulders of the fibrous cap of the plaque (i.e., at the junctions of the cap with the adjacent layer of the artery). Other authors have analysed this configuration and found similar results, usually considering two-dimensional cross-sections of the plaque [7–9]. However, there are only a few studies that look at the location of the rupture in the axial direction of the plaque, as it is more complex to measure in samples. Falk [10] reported that the stenotic plaque could rupture upstream, downstream or at the middle of the constriction, but that the precise location had not been properly analysed in coronary arteries. Later on, it was suggested that the cell composition was different between the upstream and downstream regions of the stenosis [11]. Specifically, a larger macrophage presence was observed in the upstream region and it was related to a higher vulnerability of the plaque in the upstream part. Other authors have used computational modelling to analyse the plaque stresses in the axial direction. Imoto et al. performed a finite-element analysis of an axisymmetric plaque, considering a uniform pressure at the wall [12]. The thickness of the fibrous cap impacted the location of the maximum stresses, which were usually found where the cap was thinnest. On the other hand, if the fibrous cap thickness was kept constant, the stress was not affected by a larger lipid core. Gao et al. performed a numerical analysis of three-dimensional patient-specific geometries, and reported that the maximum stress was more likely to occur in the upstream region for severe plaques [13]. In 2012, Belzacq et al. studied the influence of the plaque length or stenosis severity,

* Corresponding author.
E-mail address: donal.mcnally@nottingham.ac.uk (D. McNally).

https://doi.org/10.1016/j.medengphy.2019.02.015
1350-4533/

among other features [14]. They reported a change of the stress distribution for shorter plaques, which made them more vulnerable than longer plaques.

Other studies using fluid-structure interaction (FSI) models, including plaque modelling, analysed the influence of different factors on the maximum stresses on the wall. For example, Tang et al. studied the effect of several parameters, such as the lipid core size and the cap thickness, and reported higher stresses for thinner fibrous caps [15]. They also introduced the analysis of patient-specific geometries and found similar results, relating plaque vulnerability to large lipid cores and thin fibrous caps [16]. Other works have also linked an increase of the maximum stress levels to a decrease of the cap thickness [17,18]. By modelling the lipid core as a material with low stiffness, two-dimensional FSI simulations using a patient-specific geometry were performed by Kock et al., and observed the highest first-principal stresses at the inlet and outlet of the stenosis region [19]. A similar study by Thrysøe et al. [20] showed that the peak principal stress was located in the region proximal to the stenosis in 50% of their patients, and that the maximum stress usually occurred where the cap was thinnest. From another point of view, Yuan et al. found that the effect of material properties on the stress values was greatly dependent on cap thickness as well as location [21].

Tang et al. also published a study linking sites of plaque rupture with high plaque stresses in carotid arteries [22]. Similar results have been reported in other studies for carotid arteries [23,24], as well as for coronary arteries [25,26]. Continuing along these lines, we hypothesise that the most likely axial location of plaque rupture in a carotid artery, which may be indicated by the location of maximum stress, as suggested by the aforementioned studies [22–26], is strongly influenced by changes of the lipid core stiffness and the geometry. In the present work, we have used an FSI model and performed a systematic variation of the following features: stenosis severity, Young's modulus of the lipid core of the plaque, positive remodelling, lipid core length, and fibrous cap stiffness. We adopt an axisymmetric blood flow geometry to solve the Navier-Stokes equations, while the artery wall and the lipid core of the plaque are modelled as hyperelastic and linear elastic materials respectively. This simplified configuration makes it possible to identify the critical parameters affecting the stress distributions.

2. Methods

2.1. Geometry

The geometry considered is an axisymmetric stenosis adapted from previous studies [27–30]. The use of this idealised model of carotid artery rather than a patient-specific geometry allows a parametric analysis where we can study the influence of different features on the solid stresses. We justify the use of this model as we are aiming to capture general patterns and distribution changes rather than specific peak values. The plaque is located in the constriction, as shown in Fig. 1. The origin of the coordinate system is located at the intersection between the centre-line of the flow domain and the section of maximum constriction. The two coordinates required to define any given position are r, in the radial direction, and z in the axial direction.

The inlet diameter D is used as the reference length unit. In our simulations, we have used a diameter of $D = 7$ mm based on the typical dimensions of a human carotid artery [31,32]. The inlet and outlet sections are located at $z = -4D$ and $z = 10D$, respectively. The wall thickness is equal to $D/10$ and constant along the axial direction, outside the stenosis region.

The inner wall radius is constant and equal to $D/2$ for all z, except for the stenotic region. For $-D \leq z \leq D$, the radius is defined by

$$r(z) = \frac{D}{2}\left\{1 - \frac{1-\gamma}{2}\left[1 + \cos\left(\frac{2\pi z}{L}\right)\right]\right\} \quad (1)$$

where $L = 2D$ is the length of the stenosis and γ is the diameter ratio. In the base model, the minimum diameter D_{min} is $D/2$ and is located at $z = 0$, hence $\gamma = D_{min}/D = 0.5$. This 50% reduction in diameter leads to a 75% area constriction (also known as stenosis severity, S), which is a typical value among previous stenotic flow studies [27,28,33]. A 75% occlusion is also a medically relevant value, when surgery is usually recommended [34].

The contour of the core of the plaque follows the shape of the stenosis. The solid part between the core and the flow domain is the fibrous cap. The thickness of this cap, t_c, is constant along the plaque and equal to 100 µm, which is a typical value of plaques with thin fibrous caps [17,35,36].

Smaller severity values than the 75% of the base model are considered alongside a positive remodelling geometry. Positive remodelling consists on an expansion of the artery wall in the outward direction [37]. In particular, simulations are performed for a non-stenotic and a 25% stenotic case, and compared to the base model. In both cases, the thickness of the artery wall around the lipid core is kept constant and equal to the nominal wall thickness, t_w. In addition, the positive remodelling is assumed to keep the same shape as the stenosis, but in the outward normal direction. The geometry of the considered cases is shown in Fig. 2. It should be noted that, due to the previous assumptions, the size of the lipid core for the 25% stenotic case (defined by its thickness, h_1, in the figure) is larger than the other two (defined by the thickness h_0).

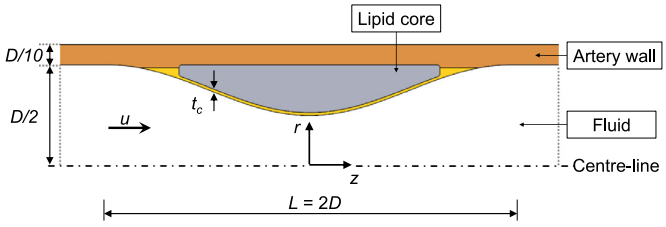

Fig. 1. Idealised axisymmetric stenosis geometry showing both the fluid and the solid domains. The origin is located at the centre line of the throat. The thickness of the artery wall is $D/10$, being D the diameter of the fluid domain.

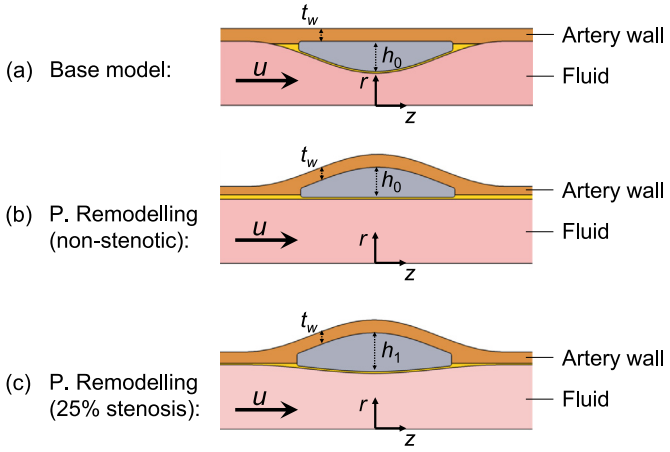

Fig. 2. Geometry of the cases in the positive remodelling analysis. (a) base model (75% stenosis); (b) non-stenotic case with positive remodelling; (c) 25% severity with positive remodelling. t_w denotes the wall thickness and it is equal in all cases. h_0 and h_1 denote the thickness of the lipid core at $z = 0$.

2.2. Governing equations and boundary conditions

2.2.1. Flow model

The blood is modelled as a Newtonian, incompressible fluid. The flow field is described by the continuity and the Navier–Stokes equations:

$$\nabla \cdot u = 0, \tag{2}$$

$$\frac{\partial u}{\partial t} + \boldsymbol{u} \cdot \nabla \boldsymbol{u} = -\frac{\nabla p}{\rho} + \nu \nabla^2 u, \tag{3}$$

where $\boldsymbol{u}$ is the fluid velocity vector, t the time, p the pressure, ρ the fluid density and ν the kinematic viscosity. The simulations are performed using $\rho = 1000\,\mathrm{kg/m^3}$ and $\nu = 4 \times 10^{-6}\mathrm{m^2/s}$, which are average values used in previous works [24,38,39].

The Reynolds number is $Re = 300$ and it is based on the inlet diameter. It is defined as $Re = UD/\nu$, where U is the sectional average inlet velocity. This value is physiologically representative and used also in previous studies of carotid arteries [5,31].

A parabolic velocity profile $\boldsymbol{u}_{\mathrm{in}} = (u_{\mathrm{in}}, 0)$ is prescribed at the inlet cross-section of the flow domain: $u_{\mathrm{in}}(r) = 2U\left[1 - 4(r/D)^2\right]$. At the outlet, an outflow pressure p_{out} equal to 160 mmHg (21.3 kPa, as used in previous studies [19]) is prescribed via a normal stress condition: $\left[-p\boldsymbol{I} + \rho\nu\left(\nabla \boldsymbol{u} + \nabla \boldsymbol{u}^T\right)\right]\boldsymbol{n} = -p_{\mathrm{out}}\boldsymbol{n}$. This condition reduces to the standard *stress-free* outflow condition if $p_{\mathrm{out}} = 0$ is chosen [27,30]. In a flow-only analysis, this value would have had no effect, since only pressure gradients affect the flow field, as shown in Eq. (3). However, due to the solid mechanics included here (i.e. we used an FSI model), it is necessary to set a specific pressure value.

2.2.2. Solid model

The artery wall is considered as a non-linear hyperelastic solid. In order to specify the different material properties, we use the nearly incompressible neo-Hookean model, which considers the following strain energy density function, W:

$$W = \frac{1}{2}\mu(I_1 - 3) + \frac{1}{2}\kappa(J_{el} - 1)^2, \tag{4}$$

where μ denotes the shear modulus, I_1 is the first invariant of the isochoric part of the elastic right Cauchy–Green deformation tensor, κ refers to the bulk modulus and J_{el} denotes the elastic volume ratio. We use the same values as in previous studies [19]: $\mu = 6\,\mathrm{MPa}$ and $\kappa = 600\,\mathrm{MPa}$. On the other hand, the lipid core is described as a linear elastic material and characterised by its Young's modulus, E_c. This value has been suggested to be around 100 times smaller than the equivalent Young's modulus of the artery wall [16,40]. We use $E_c = 100\,\mathrm{kPa}$ for the base model, with a Poisson's ratio $\nu_c = 0.49$ and a density $\rho_c = 900\,\mathrm{kg/m^3}$.

We decided to use a simple neo-Hookean model, which has been reported to be valid for small deformations [19]. Previous works in the field have also considered other hyperelastic models when defining the mechanical properties of the solid: the modified Mooney–Rivlin [16], the one proposed by Ogden [17] or the anisotropic model presented by Holzapfel–Gasser–Ogden [14].

Regarding the boundary conditions, the displacement $\boldsymbol{\xi}$ of the artery is constrained at the inlet ($\boldsymbol{\xi} = \boldsymbol{0}$), and no axial displacement is allowed at the outlet ($\xi_z = 0$). Of the different conditions tested, these were the ones which provided the most well-defined inflow and outflow. The domain lengths were varied to ensure that the stresses in the stenosis were not affected by the proximity to inflow and outflow boundaries.

2.2.3. Fluid-structure interaction coupling

Matching conditions are required at the interface between solid and fluid, to close the coupled system: the velocity continuity,

$$\boldsymbol{u} = \frac{\partial \boldsymbol{\xi}}{\partial t}, \tag{5}$$

and the stress continuity, meaning that the stresses on the wall and fluid along the interface are equal (but opposite in the outward normal direction):

$$\frac{\boldsymbol{f}}{\rho} = \boldsymbol{n} \cdot \left[-\frac{p}{\rho}\boldsymbol{I} + \nu\left(\nabla \boldsymbol{u} + \nabla \boldsymbol{u}^T\right) - \frac{2}{3}\nu(\nabla \cdot \boldsymbol{u})\boldsymbol{I}\right], \tag{6}$$

where $\boldsymbol{n}$ denotes the outward normal to the boundary.

2.3. Numerical methods

The simulations are performed with a finite element method using the COMSOL Multiphysics software. The movement of the elastic walls is achieved by using an arbitrary Lagrangian–Eulerian (ALE) method, where the solid mechanics follow a Lagrangian description while the flow field is described by an Eulerian formulation. COMSOL Multiphysics has been previously validated and used in several studies to perform blood flow simulations [41] as well as fluid-structure interaction studies of flow through elastic arteries using idealised geometries [14,17,42] and patient-specific models [19,20].

The mesh was also generated using COMSOL Multiphysics. The two-dimensional spatial domain is discretized using standard triangular/quadratic finite elements of the second order for the flow velocity and solid displacement fields, and of the first order for the pressure field (P2-P2-P1). The numerical convergence of the solver was tested with respect to grid and domain size. Specifically, a mesh convergence analysis was performed until the stress measurements were not affected by a change in the mesh resolution of more than a 0.5%. For the straight pipes upstream and downstream the stenosis region, we use a structured mesh with 12,272 elements (maximum element size $D/40$). For the constriction, due to the curved domain and complex fluid and solid mechanics, we use a finer unstructured grid, with 30,599 elements, especially for the fibrous cap, which is the region where the stress distributions will be analysed. A picture of the mesh is shown in Fig. 3.

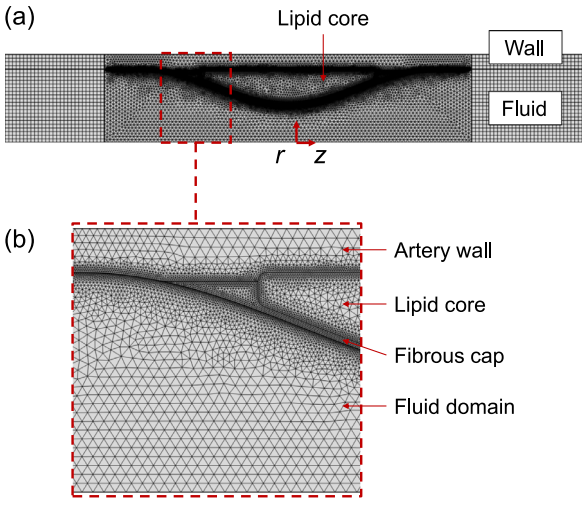

Fig. 3. (a) Representation of the mesh. (b) Detail of the stenosis region, showing the discretization of the fibrous cap.

3. Results

3.1. Effect of severity and core stiffness

We first studied the influence of both stenosis severity and plaque composition on the solid stress and wall displacements. In order to simplify the modelling of the different plaque compositions, we varied the elasticity of the lipid core by means of the Young's modulus, E_c. This way, lipid-filled plaques were modelled as linear elastic materials with a Young's modulus that was around 100 times smaller than the equivalent Young's modulus of the artery wall [16] ($E_c = 50$–100 kPa). On the other hand, calcified plaques were modelled by increasing the Young's modulus of the lipid core (up to 1000 kPa). Regarding the severity, both mild (50% occlusion) and severe (75% occlusion) cases were considered. Table 1 summarises the six different models analysed.

A general picture of the flow solution and stresses obtained from our simulation is presented in Fig. 4(a). The colours of the fluid domain denote blood velocity, u, and the colours of the solid domain refer to the first principal stress, σ_1, on the artery wall. On the other hand, the fluid pressure field is shown in Fig. 4(b).

Fig. 5(a) shows the axial distribution of the first principal stress, σ_1, along the artery wall and the fibrous cap of the plaque. In all cases, the stress outside the stenosis region was at the same level, at around 120 kPa. This value effectively corresponds to the circumferential stress at the inner wall of a equivalent thick-walled cylinder loaded by internal pressure. Near $z = \pm D$, due to the intimal thickening of the artery at the beginning of the plaque, the stress decreased reaching a minimum shortly afterwards. Then, the largest differences in the stress distribution were observed due to the lipid core, which was delimited to the region $-0.6D < z < 0.6D$.

Table 1
Stenosis severity and Young's modulus of the lipid core for each case considered. Case *E* corresponds to the base model.

Case	Stenosis severity (%)	Young's modulus of lipid core
A	50	50 kPa
B	50	100 kPa
C	50	1000 kPa
D	75	50 kPa
E	75	100 kPa
F	75	1000 kPa

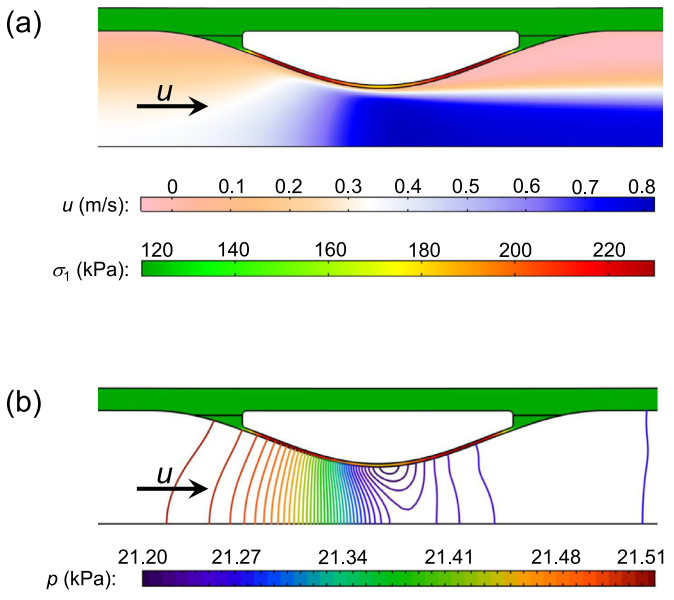

Fig. 4. (a) Flow velocity field, u, and first principal stress, σ_1, distribution on the artery wall for a steady state simulation in the region around the stenosis. (b) Flow pressure field, p, and first principal stress, σ_1.

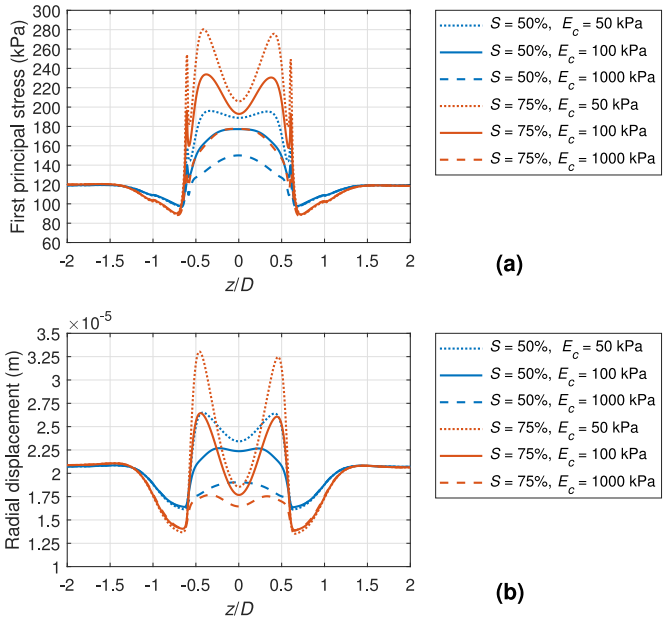

Fig. 5. Influence of stenosis severity and plaque composition on the axial distribution of (a) first principal stress and (b) radial displacements. Magnitudes measured at the interface boundary between the flow field and the wall. Results are shown for the cases presented in Table 1.

The results can be divided into two groups: on the one hand, the mild stenosis with the calcified core ($E_c = 100$–1000 kPa) along with the severe stenosis with the calcified core ($E_c = 1000$ kPa). On the other hand, the mild stenosis with the lipid-filled core ($E_c = 50$ kPa) and the severe stenosis with the lipid-filled core ($E_c = 50$–100 kPa). For the first group, the stress distribution was relatively flat, with the maximum located in the middle region of the stenosis. For the second group, the stress level increased. The distribution also changed and presented two peaks, located in the middle of the upstream and downstream regions of the stenosis. The maximum stress for the base model ($S = 75\%$, $E_c = 100$ kPa) was 30% higher than the maximum for the calcified plaque model. The variation was significant but it is important to note that the variation of the lipid core material properties was larger, since the Young's modulus decreased by an order of magnitude. For the softest core considered ($E_c = 50$ kPa) in the severe stenosis, the maximum stress was 280 kPa. This value got closer to the 300 kPa rupture threshold usually mentioned in the literature [8].

The differences in stresses were reflected as well in the radial displacement distribution (Fig. 5(b)). Indeed, the two-peak distribution characteristic of the base case and the mild and lipid-filled plaque were present. On the other hand, the cases with stiffer (calcified) plaques showed a flatter curve.

In order to explain the stress distribution, we should take into account the fluid pressure along the axial direction, as the pressure is the main contributor to the loading of the wall. The pressure did not depend on the lipid core elasticity and it was only affected by the stenosis severity. Indeed, we found a pressure drop of $\sim$ 300 Pa (equivalent to a 1.4% of the total pressure) for the 75% occlusion, while that value decreased to around 80 Pa for the 50% severity stenosis. Taking a closer look at the stress plot in Fig. 5(a), there was a slight difference in the peak stress before and after the minimum lumen section for the severe stenosis cases. This small change was approximately of 1.5%, which could be associated with this pressure drop along the plaque, as shown in Fig. 4(b).

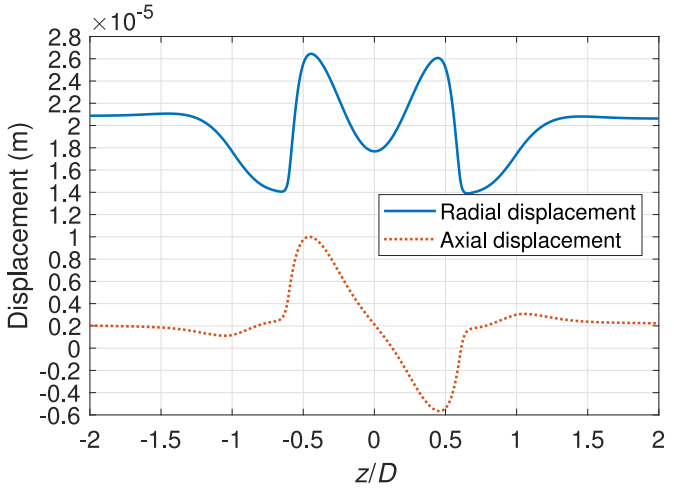

Fig. 6. Axial and radial displacements of the wall for the baseline case.

The axial displacements of the wall for the base model are relatively smaller than the radial displacements, as shown in Fig. 6. In particular, the maximum of the radial component is around 2.6 times larger than the axial one. The shape of the axial displacements curve is due to the deformation created by the fluid pressure on the wall [14], which leads to a positive peak upstream and a negative one downstream the constriction. In addition, the maximum radial and axial displacements are found at the same location. This kind of deformation is also in agreement with the experimental results reported by Choi et al. [43], who studied a pulsatile flow condition. It should be noted as well that these values are relatively small for the material properties considered in this model, with a maximum axial displacement of 10^{-5} m, or $1.4210^{-3}D$.

In summary, we have identified three different locations in the axial direction that could become sites of rupture. For the most vulnerable plaques ($S = 50\%, E_c = 50$ kPa, and $S = 75\%, E_c =$ 50- 100 kPa), the stress peaks were located approximately at the middle of the upstream and downstream regions of the stenosis respectively. For the other plaques ($S = 50\%, E_c =$ 100-1000 kPa, and $S = 75\%, E_c = 1000$ kPa), the maximum of the stress peak was close to the minimum lumen section. Finally, all cases presented a local maximum at the beginning of the lipid core region, which will be discussed further in the Discussion section. Hence, depending on the lipid composition and the stenosis severity, the rupture site could be located at three different positions.

3.2. Effect of the positive remodelling

The axial distribution of the first principal stress is presented in Fig. 7(a). The first thing to note is a 15% increment of the maximum stress in the fibrous cap for the 25% stenotic case compared to the non-stenotic one. On the other hand, the non-stenotic case presented similar stress levels in relation to the base model. Hence, the only effect of the stenosis severity seemed to be the change of the stress distribution (presenting the two peaks rather than a flat curve).

The radial displacements showed similar results (Fig. 7(b)). The two curves of the positive remodelling cases kept the same shape, showing a constant deformation along the fibrous cap. On the contrary, the base model reflected the shape of the stenosis, and the radial displacements presented a distribution similar to that of the first principal stress.

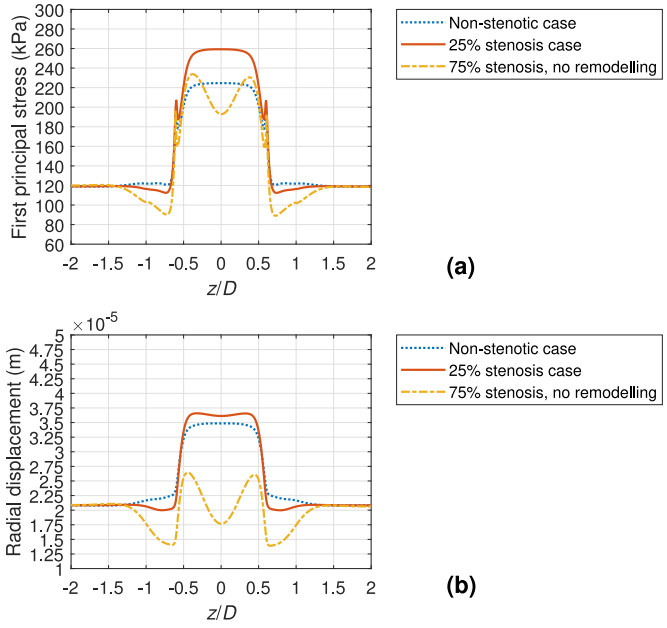

Fig. 7. Influence of the positive remodelling on the axial distribution of (a) first principal stress and (b) radial displacements. Magnitudes measured at the interface boundary between the flow field and the wall.

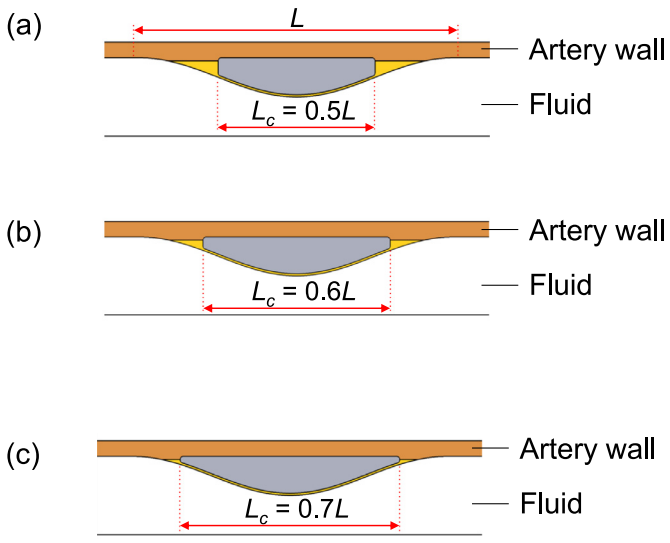

Fig. 8. Three configurations considered to analyse the influence of the lipid core length: (a) $L_c = 0.5L$, (b) $L_c = 0.6L$ (base model) and (c) $L_c = 0.7L$.

3.3. Effect of the lipid core length

The lipid core length, L_c, was varied to analyse its influence on the stress distribution. Three cases were considered: $L_c = 0.5L$ (shorter lipid), $L_c = 0.6L$ (the base model), and $L_c = 0.7L$ (longer lipid). The variation of the lipid length was carried out keeping constant the stenosis length (L), the fibrous cap and outer wall thickness, as well as the fillet radius of the core, in order to perform a uniform parametric analysis with other variables unchanged. The three cases are represented in Fig. 8.

As shown in Fig. 9(a), the axial stress distribution was remarkably different for each case. A shorter lipid core increased both the local and absolute peaks, while also affecting the gradients. These results suggest that shorter lipid cores could be more dangerous than plaques with longer cores, for the same thickness of the fibrous cap.

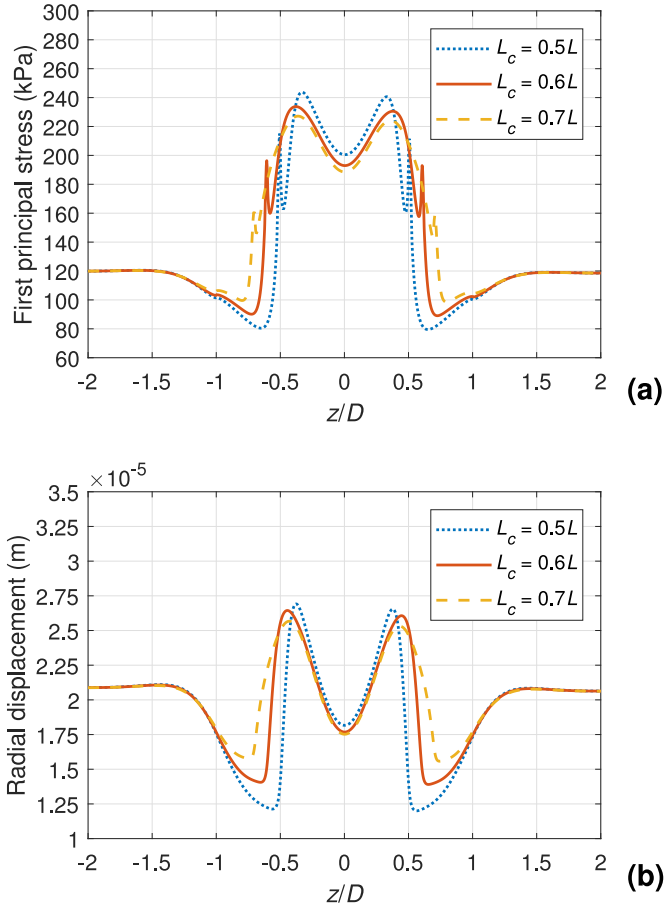

Fig. 9. Influence of the lipid core length on the axial distribution of (a) first principal stress and (b) radial displacements. Magnitudes measured at the interface boundary between the flow field and the wall.

The radial displacements, as shown in Fig. 9(b), presented a similar behaviour. Both the minima and maxima of the curves were increased for the shortest lipid core.

3.4. Effect of the cap stiffening

We considered three different values for the bulk modulus of the fibrous cap, κ_{fc}: same as the wall ($\kappa = 600$ MPa), two times larger (baseline model), and ten times larger. The axial stress distribution for different values of cap stiffness is shown in Fig. 10. As it can be seen in the figure, decreasing the cap stiffness to half the base value, or increasing it to 10 times the original value had no visible effect on the stress. The same result was observed regarding the radial displacement along the plaque.

In summary, each parametric analysis showed different effects on the stress distribution. The plaque composition and the positive remodelling of the artery were found to be the most important parameters, as they had the largest effect on the absolute peak values, while also changing the axial distribution along the fibrous cap. On the other hand, the local stress peaks were especially affected by the length of the lipid core, as those values increased when the core length decreased. Finally, the stiffening of the fibrous cap did not impact the stress distribution for the range of values considered in this work.

4. Discussion

Before proceeding with the analysis of the results, we would like to justify the use of a steady flow instead of a pulsatile one.

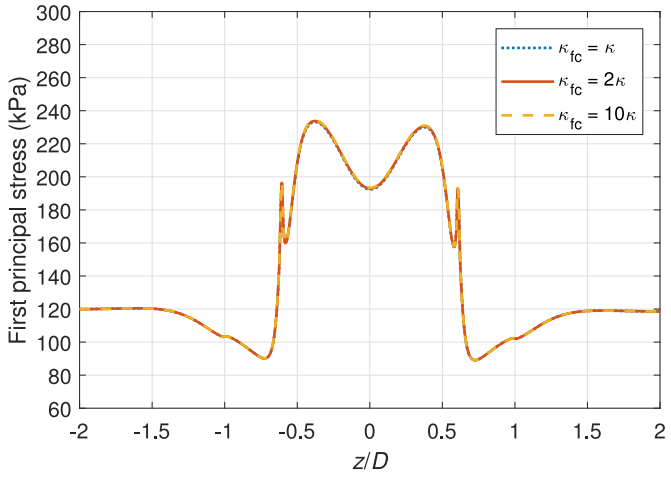

Fig. 10. Influence of the cap stiffening on the axial distribution of first principal stresses. Magnitudes measured at the interface boundary between the flow field and the wall.

When the heart beats, the contraction during the systole creates a pressure wave that travels along the arterial tree. The velocity of propagation of these pressure waves is the pulse wave velocity, *PWV* [44]. According to Pereira et al., the pulse wave velocity in the carotid artery is in the range of $PWV = 3$–12 m/s. Therefore, the minimum wavelength is 3 m, considering that the heart typically beats once a second. Since the pressure wavelength is more than 30 times larger than the domain length, the local non-stationary effects on the wall could be neglected. We tested this assumption by performing a simulation of a pulsatile inflow case, with a 1-second period. The significant changes of the pressure values during the period (up to a 40% from the average values) led to similar changes of the stress levels, but the distribution was essentially the same. This pattern was constant over the following periods. Indeed, the peak value of the stress distributions at the same time for different periods did not change significantly, staying constant and varying less than a 0.01%. Therefore, we have used a steady inflow with a systolic pressure value (maximum pressure during the period), considering the most critical conditions during the period.

The combined analysis of the stenosis severity and plaque composition shows that both effects should be considered simultaneously. Significant differences in the stress levels are observed for both severe and mild stenoses, depending on the stiffness of the lipid core. Indeed, plaque rupture is considered to be more dependent on the plaque composition rather than stenosis severity [10], as the stress along the fibrous cap increases when the lipid stiffness is lowered.

The novelty of our work is related to the effect of stenosis severity and lipid core stiffness on the the stress curve, which varies from a flat shape to a two-peak distribution. A similar change was reported by Belzacq et al. [14], when varying the plaque length (rather than the lipid composition), so they reported it as a ‘pinching effect’. Since we used a constant plaque length, the change in the stress distribution is related to the lipid core stiffness, which was kept constant in their study. This result implies that the change of the lipid composition may impact the stress values significantly, but only when the change of stiffness is large enough. Small increases of the Young’s modulus do not produce a noticeable effect on the stress peaks, which is in agreement with previously published results [16,45], but changing the Young’s modulus by an order of magnitude has noticeable effects on the stress.

It is worth mentioning about the local peaks of stress at the beginning and at the end of the lipid core region ($z \simeq \pm 0.6D$,

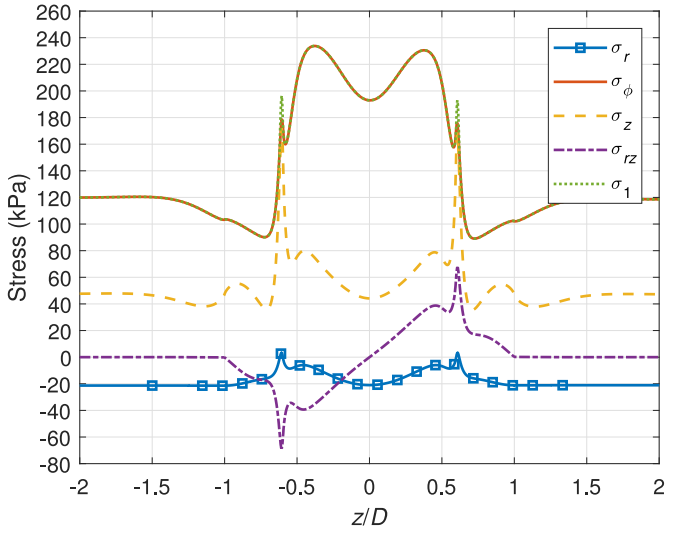

Fig. 11. Axial distribution of the components of the stress tensor for the base model (75% stenosis, $E_c = 100$ kPa). σ_r, σ_ϕ and σ_z denote the radial, circumferential and axial components respectively; σ_{rz} the shear stress component; and σ_1 the first principal stress.

Fig. 5(a)). These peaks are largely influenced by the chosen shape of the lipid core ends. The sudden change of thickness of the wall sustaining the loading (from the thickened wall to the fibrous cap with a lipid core), leads to this local change of the stress. It has been suggested that sometimes the rupture occurs at points of local stress concentrations, but not at the absolute maximum stress location [46]. These local maxima could indicate one of those plaque rupture sites. The local maxima occur at the ends of the plaque while the global maxima occur closer to the middle. This could help to explain, from a mechanical point of view, why the axial rupture location has not been precisely defined, as reported by Falk [10].

In addition to the first principal stress, the shear stress was also examined to check if it was a limiting factor in the plaque rupture process. A graph showing all the non-zero components of the stress tensor for the base model is given in Fig. 11. Several points should be noted here: (1) the shear components of the stress tensor $\sigma_{r\phi}$ and $\sigma_{\phi z}$ were equal to zero (due to the axisymmetry). (2) The remaining component σ_{rz} was zero outside the stenosis region, but it presented two peaks of 70 kPa at $z = \pm 0.6D$, corresponding to the ends of the lipid core. (3) The circumferential component, σ_ϕ, matched the first principal stress distribution almost perfectly, except at the lipid core ends ($z = \pm 0.6D$). At these locations, the axial component, σ_z, seemed to be as important as the circumferential component stress. (4) According to the Tresca criterion, the shear strength of an isotropic material is half the tensile yield strength. Our results show that the shear stress magnitude was always smaller than half the first principal stress. We concluded that, although significant at $z = \pm 0.6D$, the shear stress seemed to not be the main contributor to the plaque rupture process.

The positive remodelling study showed some interesting results. As shown in Fig. 7, the average stress levels in the stenosis region are similar between the base model and the non-stenotic positive remodelling case. There is, however, a change in the stress distribution, which could eventually lead to different rupture sites. This change in stress distribution is attributed to the difference in the fluid pressure distribution. Indeed, the stenotic case presents a sudden pressure drop due to the constriction, which affects the stress distribution accordingly. A combination of a positive remodelling effect and a mild stenosis (the 25% case in the same analysis) has a great effect on the overall stress in the fibrous cap. The peak stress increases by 11% in the mild stenotic case compared to the base model, reaching a maximum of 259 kPa. This magnitude is also closer to the 300 kPa rupture threshold [8]. It should be noted however that the mild stenotic case is the geometry with the larger lipid core, greatly impacting the stress distribution.

It should be noted that although the 75% stenotic case and the non-stenotic model with positive remodelling share similar stress levels (with a different distribution), their radial displacement values are different (Fig. 7(b)). Two factors could explain this result: on the one hand, due to the larger constriction at $z = 0$, the fluid pressure for the 75% stenotic case is lower than the models with positive remodelling, therefore affecting the radial displacement; on the other hand, the severe stenotic geometry may be less prone to radial deformation. In particular, the 75% stenotic case is deformed in both the radial and axial directions due to the shape of the wall, while the positive remodelling cases are mainly deformed in the radial direction only.

The results from the analysis of the lipid core length showed that, interestingly, the highest stress peaks are found for the shortest core (Fig. 9). Since we varied the lipid length at constant thickness of the fibrous cap and outer wall, the shortest plaque case is subjected to the minimum stress outside the lipid region, where the wall is thickest. This thickness change at the beginning of the fibrous cap creates a sudden increase of the stress levels, and thus the local maxima are also remarkably higher than in the other cases (17–31%).

The axial distribution of stress resembles that of the plaque composition analysis as shown in Fig. 5. Two peaks appear at the middle of the upstream and downstream regions of the stenosis, and smaller, local peaks at the beginning and end of the lipid core region. Two possible sites of rupture are identified: the first one related to the global maxima in the stress distribution, and others at the beginning and end of the lipid region. The latter should be especially important in longitudinally short plaques.

The influence of the lipid core size was studied by Tang et al. [15], but we cannot make a direct comparison as in their study the fibrous cap thickness was variable and that has a great impact on the stress values. Indeed, the stress levels decreased for a smaller lipid pool, but the cap thickness was larger than their baseline model. On the other hand, it is interesting to compare our results to the ones obtained by Cilla et al. [36]. They performed a parametric variation of the lipid core length, and analysed the peak stress at the minimum lumen section, where the cap thickness was constant. They reported that the stress remained approximately constant (varying less than 10 kPa). On our simulations, we found a significant variation of stress distribution when varying the lipid core length, but at $z = 0$ (minimum lumen section) the value stayed relatively constant for the three cases considered, within the 10 kPa range (Fig. 9). Hence, our results are in agreement with those by Cilla et al. [36] at $z = 0$. However, here we have analysed the whole axial distribution, and observed that the stress maxima and distributions vary significantly with the core length.

It should be noted that the effect of the lipid length is less than that due to the change of lipid stiffness and stenosis severity. Indeed, when varying the lipid stiffness, we observe a 20% increase of the maximum stress value with respect to the base model. When analysing the effect of the lipid length, the maximum stress increases only by a 4.3%. On the other hand, the local maxima are more affected by the lipid core length: the shortest lipid presents a local peak that is 34% larger than the longest one.

We observed no significant differences in the stress distribution when varying the fibrous cap stiffness. Some authors have reported that the fibrous cap stiffness is 2–5 times larger than that of the healthy artery wall [47]. Our results imply that for the material properties and geometry considered in this analysis, the stiffening

of the fibrous cap does not influence the stress distribution noticeably. This behaviour could be explained by comparing the current geometry with a thin-walled pressurised tube. In that case, the circumferential stress does not depend on the material properties of the wall, so that could explain why the change of stiffness of the fibrous cap does not change the stress levels. Therefore, the effect of the plaque composition along with the stenosis severity as well as the lipid core length are considered more crucial factors when analysing possible sites of rupture.

Finally, it should be acknowledged the limitation of not considering the axial stretch of the artery. This may have an effect on the results, but the stretch was not considered in this case due to the idealised nature of the geometry and the parametric analysis performed.

5. Conclusions

Simulations of incompressible, steady flow through an axisymmetric stenosed artery have been performed to systematically vary the mechanical parameters in the plaque and analyse the effects of the axial distribution of stresses. In particular, we have investigated: the stenosis severity, the lipid core stiffness, the positive remodelling of the artery, the lipid core length and the fibrous cap stiffness. Our goal was to analyse the importance of these parameters on the axial distributions of stress, and to identify possible rupture locations in the axial direction.

We found that the degree of stenosis and the lipid core stiffness, along with the positive remodelling, had the largest effect on the peak values. The stress distribution also changed significantly, especially with the lipid core stiffness, from a one-peak curve (for calcified cores) to a two-peak curve (for lipid-filled plaques). In addition, shorter lipid cores with a significant change of wall thickness (larger than the equivalent for longer lipid cores) resulted in higher maximum stresses, both absolute and local. On the contrary, varying the stiffness of the fibrous cap did not influence the axial distributions. From these results, we have identified potential sites of plaque rupture for each case: the midpoints of the upstream and downstream regions of the stenosis (for severe, lipid-filled plaques), the ends of the lipid core (for longitudinally short cores), and the middle of the stenosis (for mild stenoses with positive remodelling).

As future work, three-dimensional simulations would allow to incorporate the effects of multi-directional flow and eccentric plaques. Finally, if possible, it would be interesting to investigate axial rupture locations in patient-specific geometries.

Conflict of interests

None declared.

Ethical approval

Not required.

Acknowledgments

O. Tammisola gratefully acknowledges the support from Swedish Research Council under grant VR2013-5789.

References

[1] Lusis AJ. Atherosclerosis. Nature 2000;407:233–41. doi:10.1038/35025203.
[2] Taylor CA, Figueroa CA. Patient-specific modeling of cardiovascular mechanics. Ann Rev Biomed Eng 2009;11:109–34. doi:10.1146/annurev.bioeng.10.061807.160521.
[3] Razavi A, Shirani E, Sadeghi MR. Numerical simulation of blood pulsatile flow in a stenosed carotid artery using different rheological models. J Biomech 2011;44(11):2021–30. doi:10.1016/j.jbiomech.2011.04.023.
[4] Weber C, Noels H. Atherosclerosis: current pathogenesis and therapeutic options. Nat Med 2011;17(11):1410–22. doi:10.1038/nm.2538.
[5] Ku DN, Giddens DP, Zarins CK, Glagov S. Pulsatile flow and atherosclerosis in the human carotid bifurcation. Positive correlation between plaque location and low oscillating shear stress. Arterioscler Thromb Vasc Biol 1985;5(3):293–302. doi:10.1161/01.ATV.5.3.293.
[6] Richardson PD, Davies M, Born G. Influence of plaque configuration and stress distribution on fissuring of coronary atherosclerotic plaques. Lancet 1989;334(8669):941–4. doi:10.1016/S0140-6736(89)90953-7.
[7] Loree HM, Kamm RD, Stringfellow RG, Lee RT. Effects of fibrous cap thickness on peak circumferential stress in model atherosclerotic vessels. Circ Res 1992;71:850–8. doi:10.1161/01.RES.71.4.850.
[8] Cheng GC, Loree HM, Kamm RD, Fishbein MC, Lee RT. Distribution of circumferential stress in ruptured and stable atherosclerotic lesions. A structural analysis with histopathological correlation. Circulation 1993;87(4):1179–87. doi:10.1161/01.CIR.87.4.1179.
[9] Kumar RK, Balakrishnan KR. Influence of lumen shape and vessel geometry on plaque stresses: possible role in the increased vulnerability of a remodelled vessel and the “shoulder” of a plaque. Heart (Br Card Soc) 2005;91(11):1459–65. doi:10.1136/hrt.2004.049072.
[10] Falk E. Why do plaques rupture? Circulation 1992;86(6 Suppl):III30–42. http://www.ncbi.nlm.nih.gov/pubmed/1424049.
[11] Dirksen MT, Van Der Wal AC, van den Berg FM, van der Loos CM, Becker aE. Distribution of inflammatory cells in atherosclerotic plaques relates to the direction of flow. Circulation 1998;98(19):2000–3. doi:10.1161/01.CIR.98.19.2000.
[12] Imoto K, Hiro T, Fujii T, Murashige A, Fukumoto Y, Hashimoto G, et al. Longitudinal structural determinants of atherosclerotic plaque vulnerability: a computational analysis of stress distribution using vessel models and three-dimensional intravascular ultrasound imaging. J Am Coll Cardiol 2005;46(8):1507–15. doi:10.1016/j.jacc.2005.06.069.
[13] Gao H, Long Q, Kumar Das S, Halls J, Graves M, Gillard JH, et al. Study of carotid arterial plaque stress for symptomatic and asymptomatic patients. J Biomech 2011;44(14):2551–7. doi:10.1016/j.jbiomech.2011.07.012.
[14] Belzacq T, Avril S, Leriche E, Delache A. A numerical parametric study of the mechanical action of pulsatile blood flow onto axisymmetric stenosed arteries. Med Eng Phys 2012;34(10):1483–95. doi:10.1016/j.medengphy.2012.02.010.
[15] Tang D, Yang C, Kobayashi S, Ku DN. Effect of a lipid pool on stress/strain distributions in stenotic arteries: 3-D fluid-structure interactions (FSI) models.. J Biomech Eng 2004;126(3):363–70. doi:10.1115/1.1762898.
[16] Tang D, Yang C, Zheng J, Woodard PK, Sicard GA, Saffitz JE, et al. 3D MRI-based multicomponent FSI models for atherosclerotic plaques. Ann Biomed Eng 2004;32(7):947–60. doi:10.1023/B:ABME.0000032457.10191.e0.
[17] Li Z-Y, Howarth SPS, Tang T, Gillard JH. How critical is fibrous cap thickness to carotid plaque stability? A flow-plaque interaction model. Stroke 2006;37(5):1195–9. doi:10.1161/01.STR.0000217331.61083.3b.
[18] Gao H, Long Q, Graves MJ, Gillard JH, Li Z-Y. Carotid arterial plaque stress analysis using fluid-structure interactive simulation based on in-vivo magnetic resonance images of four patients. J Biomech 2009;42(10):1416–23. doi:10.1016/j.jbiomech.2009.04.010.
[19] Kock SA, Nygaard JV, Eldrup N, Fründ ET, Klærke A, Paaske WP, et al. Mechanical stresses in carotid plaques using MRI-based fluid-structure interaction models. J Biomech 2008;41(8):1651–8. doi:10.1016/j.jbiomech.2008.03.019.
[20] Thrysøe SA, Oikawa M, Yuan C, Eldrup N, Klærke A, Paaske WP, et al. Longitudinal distribution of mechanical stresses in carotid plaques of symptomatic patients. Stroke 2010;41(5):1041–3. doi:10.1161/STROKEAHA.109.571588.
[21] Yuan J, Teng Z, Feng J, Zhang Y, Brown AJ, Gillard JH, et al. Influence of material property variability on the mechanical behaviour of carotid atherosclerotic plaques: A 3D fluid-structure interaction analysis. Int J Numer Methods Biomed Eng 2015;31(8):e02722.
[22] Tang D, Teng Z, Canton G, Yang C, Ferguson M, Huang X, et al. Sites of rupture in human atherosclerotic carotid plaques are associated with high structural stresses: An in Vivo MRI-based 3D fluid-structure interaction study. Stroke 2009;40(10):3258–63. doi:10.1161/STROKEAHA.109.558676.
[23] Teng Z, Canton G, Yuan C, Ferguson M, Yang C, Huang X, et al. 3D critical plaque wall stress is a better predictor of carotid plaque rupture sites than flow shear stress: An in vivo MRI-based 3D FSI study. J Biomech Eng 2010;132(3):031007. doi:10.1115/1.4001028.
[24] Gao H, Long Q, Das SK, Sadat U, Graves M, Gillard JH, et al. Stress analysis of carotid atheroma in transient ischemic attack patients: evidence for extreme stress-induced plaque rupture. Ann Biomed Eng 2011;39(8):2203–12. doi:10.1007/s10439-011-0314-5.
[25] Huang X, Yang C, Zheng J, Bach R, Muccigrosso D, Woodard PK, et al. Higher critical plaque wall stress in patients who died of coronary artery disease compared with those who died of other causes: A 3D FSI study based on ex vivo MRI of coronary plaques. J Biomech 2014;47(2):432–7. doi:10.1016/j.jbiomech.2013.11.007. NIHMS150003.
[26] Costopoulos C, Huang Y, Brown AJ, Calvert PA, Hoole SP, West NE, et al. Plaque rupture in coronary atherosclerosis is associated with increased plaque structural stress. JACC: Cardiovasc Imag 2017;10(12):1472–83. doi:10.1016/j.jcmg.2017.04.017.
[27] Sherwin SJ, Blackburn HM. Three-dimensional instabilities and transition of steady and pulsatile axisymmetric stenotic flows. J Fluid Mech 2005;533:297–327. doi:10.1017/S0022112005004271.
[28] Varghese SS, Frankel SH, Fischer PF. Direct numerical simulation of stenotic flows. Part 1. Steady flow. J Fluid Mech 2007;582:253–80. doi:10.1017/S0022112007005848.

[29] Griffith MD, Leweke T, Thompson MC, Hourigan K. Effect of small asymmetries on axisymmetric stenotic flow. J Fluid Mech 2013;721:1–11. doi:10.1017/jfm.2013.109.
[30] Samuelsson J, Tammisola O, Juniper MP. Breaking axi-symmetry in stenotic flow lowers the critical transition Reynolds number. Phys Fluids 2015;27:104103. doi:10.1063/1.4934530.
[31] Perktold K, Rappitsch G. Computer simulation of local blood flow and vessel mechanics in a compliant carotid artery bifurcation model. J Biomech 1995;28(7):845–56. doi:10.1016/0021-9290(95)95273-8.
[32] Mao X, Sherwin SJ, Blackburn HM. Transient growth and bypass transition in stenotic flow with a physiological waveform. Theor Comput Fluid Dyn 2011;25(1):31–42. doi:10.1007/s00162-009-0167-9.
[33] Mao X, Blackburn HM, Sherwin SJ. Optimal inflow boundary condition perturbations in steady stenotic flow. J Fluid Mech 2012;705:306–21. doi:10.1017/jfm.2012.58.
[34] Ku DN. Blood flow in arteries. Ann Rev Fluid Mech 1997;29:399–434. doi:10.1146/annurev.fluid.29.1.399.
[35] Thrysøe SA, Stegmann AF, Eldrup N, Klærke A, Paaske WP, Kim WY, et al. The effect of carotid plaque morphology on longitudinal fibrous cap stress levels. World J Mech 2012;2(4):216–23. doi:10.4236/wjm.2012.24026.
[36] Cilla M, Borrás I, Peña E, Martínez MA, Malvè M. A parametric model for analysing atherosclerotic arteries: on the FSI coupling. Int Commun Heat Mass Transf 2015;67:29–38. doi:10.1016/j.icheatmasstransfer.2015.06.017.
[37] Badimon L, Vilahur G. Thrombosis formation on atherosclerotic lesions and plaque rupture. J Intern Med 2014;276(6):618–32. doi:10.1111/joim.12296.
[38] Tang D, Yang C, Kobayashi S, Zheng J, Vito RP. Effect of stenosis asymmetry on blood flow and artery compression: a three-dimensional fluid-structure interaction model. Ann Biomed Eng 2003;31(10):1182–93. doi:10.1114/1.1615577.
[39] Tezduyar TE, Sathe S, Cragin T, Nanna B, Conklin BS, Pausewang J, et al. Modelling of fluid-structure interactions with the space-time finite elements: arterial fluid mechanics. Int J Numer Methods Fluids 2007;54(6-8):901–22. doi:10.1002/fld.1443.
[40] Loree HM, Tobias BJ, Gibson LJ, Kamm RD, Small DM, Lee RT. Mechanical properties of model atherosclerotic lesion lipid pools. Arteriosc Thromb: J Vasc Biol 1994;14(2):230–4. doi:10.1161/01.ATV.14.2.230.
[41] Lorenzini G, Casalena E. CFD analysis of pulsatile blood flow in an atherosclerotic human artery with eccentric plaques. J Biomech 2008;41(9):1862–70. doi:10.1016/j.jbiomech.2008.04.009.
[42] Xiong H, Liu X, Tian X, Pu L, Zhang H, Lu M, et al. A numerical study of the effect of varied blood pressure on the stability of carotid atherosclerotic plaque. Biomed Eng OnLine 2014;13(152):1–13. doi:10.1186/1475-925X-13-152.
[43] Choi W, Park JH, Byeon H, Lee SJ. Flow characteristics around a deformable stenosis under pulsatile flow condition. Phys Fluids 2018;30(1). doi:10.1063/1.5009063.
[44] Pereira T, Correia C, Cardoso J. Novel methods for pulse wave velocity measurement. J Med Biol Eng 2015;35(5):555–65. doi:10.1007/s40846-015-0086-8.
[45] Ferrara A, Pandolfi A. Numerical modelling of fracture in human arteries. Comput Methods Biomech Biomed Eng 2008;11(5):553–67. doi:10.1080/10255840701771743.
[46] Tang D, Yang C, Zheng J, Woodard PK, Saffitz JE, Petruccelli JD, et al. Local maximal stress hypothesis and computational plaque vulnerability index for atherosclerotic plaque assessment. Ann Biomed Engi 2005;33(12 SPEC. ISS.):1789–801. doi:10.1007/s10439-005-8267-1.
[47] Brown DL. Cardiovascular Plaque Rupture. Marcel Dekker; 2002. ISBN:9780824702762, http://www.tandfebooks.com/action/showBook?doi=10.3109/9780203908914.